"Structural Investigation of Substituent Effect on Hydrogen Bonding in (S)-Phenylglycine Amide Benzaldimines"

George, Fanny ; Norberg, Bernadette ; Wouters, Johan ; Leyssens, Tom

Abstract

A detailed structural analysis of 23 new crystal structures of (S)-phenylglycine amide benzaldimines with various substituents (CH3, Ph, OCH3, F, Cl, Br, NO2) on the benzylidene is performed in this contribution. These compounds belong to the highly studied family of Schiff bases. Etter's nomenclature and Hirshfeld surfaces are used to describe respectively the strong hydrogen bonds and the secondary interactions existing in these compounds. Surprisingly, all 23 obtained structures can be sorted into five types according to their hydrogen bonding motifs. The potential interplay of steric and electronic effects of the substituents on the resulting bonding patterns, conformational features and packing was investigated. Our analysis revealed that neither mesomeric/inductive factors of halogens nor π-π stacking, C-H···π, and other hydrophobic interactions affect the structural outcome. The type affiliation is rather due to the interplay of three parameters: (1) the number of strong...

Document type : *Article de périodique (Journal article)*

CRYSTAL GROWTH & DESIGN

Article

pubs.acs.org/crystal

Structural Investigation of Substituent Effect on Hydrogen Bonding in (*S*)-Phenylglycine Amide Benzaldimines

Fanny George,[†] Bernadette Norberg,[‡] Johan Wouters,[‡] and Tom Leyssens*[,†]

[†]Institute of Condensed Matter and Nanosciences, Université Catholique de Louvain, 1348 Louvain-la-Neuve, Belgium

[‡]Unité de Chimie Physique, Théorique et Structurale, University of Namur, Namur, Belgium

Supporting Information

ABSTRACT: A detailed structural analysis of 23 new crystal structures of (*S*)-phenylglycine amide benzaldimines with various substituents (CH_3, Ph, OCH_3, F, Cl, Br, NO_2) on the benzylidene is performed in this contribution. These compounds belong to the highly studied family of Schiff bases. Etter's nomenclature and Hirshfeld surfaces are used to describe respectively the strong hydrogen bonds and the secondary interactions existing in these compounds. Surprisingly, all 23 obtained structures can be sorted into five types according to their hydrogen bonding motifs. The potential interplay of steric and electronic effects of the substituents on the resulting bonding patterns, conformational features and packing was investigated. Our analysis revealed that neither mesomeric/inductive factors of halogens nor $\pi-\pi$ stacking, C−H···π, and other hydrophobic interactions affect the structural outcome. The type affiliation is rather due to the interplay of three parameters: (1) the number of strong hydrogen bonds forming the motif (thermodynamic factor), (2) the ease with which the motif is formed (kinetic factor), and (3) the capacity of the motif to accommodate substituents on the different positions (steric factor). It was thus possible to suggest a stability ranking of the five structural types and to identify stable forms when polymorphism was encountered.

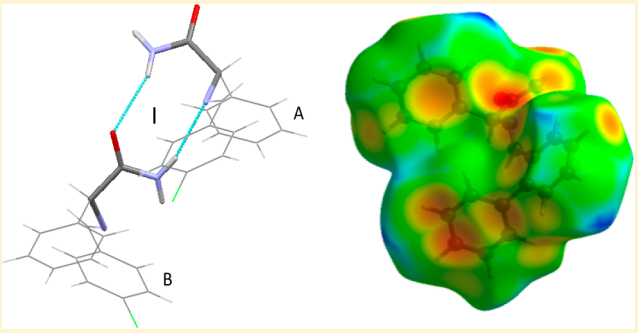

INTRODUCTION

During the past few years, Schiff bases have received much attention due to their wide range of biological activities[1,2] and industrial applications. Among their pharmacological properties, they show antibacterial,[3] anticancer,[4] antifungal,[5] and radical scavenging[6] activities. They can also be used as enzymatic intermediates or inhibitors.[7] Stable and easily synthesized, chiral Schiff bases are widely used in organic chemistry as intermediates in the formation of chiral amines and various carbonyl compounds. Because of the π-acceptor properties of the imine nitrogen, they are commonly encountered ligands in coordination chemistry.[8,9] Furthermore, they have shown their use in asymmetric catalysis.[10] Among Schiff bases, *N*-(2-methylbenzylidene)phenylglycine amide has recently been used as a model compound for deracemization through abrasive grinding,[11−15] while 2-(benzylideneamino)-2-(2-chlorophenyl)acetamide helped to demonstrate the possibility of using attrition-enhanced deracemization in an up-scaled process.[16] Both these compounds fulfill the requirements for the deracemization technique to work; they form racemic conglomerates in the solid phase (i.e., R and S molecules crystallize in different crystals), and they are easily racemizable in solution.

Schiff bases have extensively been structurally characterized,[17−22] but only a limited amount of studies have investigate the relationship between supramolecular motifs and nature/position of different substituents on a molecular framework.[23,24]

In the current contribution, we analyze the crystal structures of 20 (*S*)-phenylglycine amide benzaldimines having various substituents located on different positions on the benzylidene. This study will help to understand the solid state behavior of this type of imine and yield insight into how the nature, size, and position of the substituent impact the hydrogen bonding patterns.

All compounds were synthesized by condensation of (*S*)-phenylglycine amide ((*S*)-PGA) and the corresponding monosubstituted benzaldehyde (Scheme 1). Etter's nomenclature[25] was used to describe the strong hydrogen bonds existing in the t23 crystal structures presented here, while Hirshfeld surfaces[26] served to identify their secondary interactions. The potential interplay of steric and electronic effects of the substituents on the resulting bonding patterns, conformational features and packing was investigated in detail.

EXPERIMENTAL SECTION

Starting Materials. (*S*)-Phenylglycine amide, 2-anisaldehyde, 3-anisaldehyde, 3-nitrobenzaldehyde, and 4-nitrobenzaldehyde were

Received: May 6, 2015
Revised: June 22, 2015
Published: June 25, 2015

DOI: 10.1021/acs.cgd.5b00621
Cryst. Growth Des. 2015, 15, 4005−4019

Scheme 1. Synthesis of (*S*)-Phenylgycine Derivatives (3) by Condensation of (*S*)-PGA (1) and a Monosubstituted Benzaldehyde (2), in Dichloromethane at Room Temperature[a]

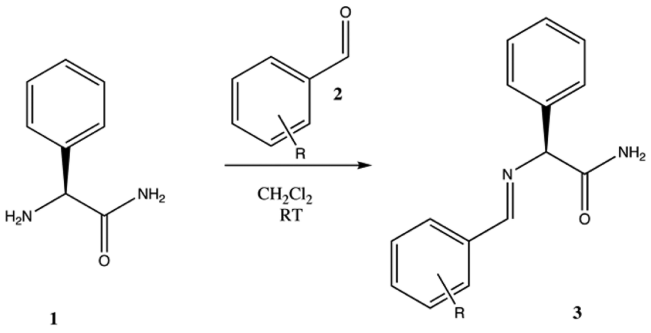

[a]R = CH_3, Ph, OCH_3, F, Cl, Br, NO_2.

purchased from Acros Organics. 2-Tolualdehyde, 3-tolualdehyde, 4-tolualdehyde, 2-bromobenzaldehyde, 3-bromobenzaldehyde, 2-chlorobenzaldehyde, 4-chlorobenzaldehyde, 3-fluorobenzaldehyde, 4-chlorobenzaldehyde, and biphenyl-2-carboxaldehyde were purchased from Sigma-Aldrich. 4-Anisaldehyde and 2-fluorobenzaldehyde were purchased from Alfa Aesar. 4-Bromobenzaldehyde and 2-nitrobenzaldehyde were purchased from Maybridge. 3-Chlorobenzaldehyde and biphenyl-4-carboxaldehyde were purchased from TCI.

Synthesis. (*S*)-PGA-aldimines were prepared by the addition of the substituted benzaldehyde to a suspension of (*S*)-PGA in dichloromethane and left to stir overnight at room temperature, as described by Dalmolen et al.[27]

Single Crystals. Most single crystals were grown by slow evaporation of the corresponding solution or by cooling crystallization to 3 °C. Different solvents (methanol, acetonitrile, ethyl acetate, dichloromethane, and acetone) were used as polymorphism was suspected for some compounds (see below). For the 2-chlorobenzaldehyde derivative, different polymorphs were obtained when using acetonitrile, acetone, or methanol as crystallization solvent. Those were named FI, FII, and FIII respectively. Similarly, two polymorphs were isolated for the 2-anisaldehyde product when using methanol and dichloromethane, and named FI and FII respectively.

Single Crystal X-ray Diffraction. Single crystal X-ray diffraction was performed on a Gemini Ultra R system (4-circle kappa platform, Ruby CCD detector) using Cu Kα radiation (λ = 1.54056 Å). Cell parameters were estimated from a pre-experiment run and full data sets collected at room temperature. The structures were solved by direct methods with the SHELXS-97 program and then refined on $|F|^2$ using SHELXL-97 software.[28] The final reported R_1 value is calculated on $|F|$ for the observed reflections ($I > 2\sigma(I)$). Non-hydrogen atoms were anisotropically refined, and the hydrogen atoms in the riding mode with isotropic temperature factors were fixed at 1.2 times U(eq) of the parent atoms (1.5 times for methyl groups). Hydrogen atoms implicated in H-bonds were located in the Fourier difference maps and freely refined.

Hirshfeld Surfaces. Hirshfeld surfaces are among other techniques[29] that allow the visualization of intermolecular interactions formed by a molecule in a given crystal structure.

The Hirshfeld surface of a molecule in a crystal is the surface delimiting "the region where the electron distribution of a sum of spherical atoms for the molecule dominates the corresponding sum over the crystal".[26] This surface can be mapped with different functions. Here, we used only the Hirshfeld surface mapped with d_e (distance external to the surface), the distance from the surface to the nearest nucleus in another molecule, which gives information on close intermolecular contacts. The surface color reflects the proximity of the neighbors: 0.55 Å (red) − 1.5 Å (green) − 2.4 Å (blue). Hydrogen bonds are visible on the d_e surface as large red regions adjacent to the H bond acceptor and as smaller orange-red dot adjacent to the H bond donor.

A two-dimensional (2D) fingerprint plot is a plot of d_e in function of d_i, the distance from the surface to the nearest atom in the molecule itself (distance internal to the surface). It summarizes all the intermolecular interactions in a given crystal and provides the relative area of the surface corresponding to each such interaction. Points are colored from blue, corresponding to the smallest nonzero contribution to the total surface, to red, for contribution of 0.1% or greater to the total surface.

Hirshfeld surfaces and 2D fingerprint plots were generated using the licensed free-of-charge CrystalExplorer software.[30]

RESULTS

All 20 synthesized aldimines are labeled according to the nature (CH_3, Ph, OCH_3, F, Cl, Br, NO_2) and position (ortho, meta, para) of the substituent on the benzylydene. They were structurally characterized through single crystal analysis. Crystallographic parameters of all compounds are displayed in Table 1. The crystal structure of o-Me at 208 K has already been reported in the CSD[31,32] and shows similar parameters.

Overall, in every structure type, the imine adopts a trans configuration with respect to the C═N bond. Moreover, except for what we will define later as type IV structures, the amide hydrogen H2B always faces the imine nitrogen N1 (Figure 1). In type IV structures, the carbonyl occupies this position. Although this might seem unfavorable due to the proximity of the lone pairs of the carbonyl and imine groups, this orientation allows H2B to form a hydrogen bond with the imine nitrogen in an intermolecular way. This conformation and the overall hydrogen bonding pattern of type IV structures also occurs in 2-(benzylideneamino)-2-(2-chlorophenyl)-acetamide, which is the only related structure reported in the CSD.[33]

A further general feature is the presence of the substituents in ortho and meta positions on the H7 side and not on the imine nitrogen side. This conformation is expected to be favored, as most of the hydrogen bonding partners are located on the nitrogen side, and substituents on this side would prevent strong hydrogen bonding interaction due to steric effects. Furthermore, ortho-substituents on the nitrogen side would lead to steric hindrance between the substituent and the nitrogen lone pair.

The only exception to the above observation is m-F for which some rotational disorder around the C1−C7 bond can be found, with about 75% of all molecules having the fluorine on the C3 atom (H7 side) and 25% on the C5 (nitrogen side). This can be explained by the small size of the fluorine atom and the reduced steric effect.

Surprisingly, we were able to categorize all 23 obtained structures (20 different compounds and respective polymorphs) in five structurally based types, according to their main hydrogen bonding motifs. The structural analysis below uses graph sets[25] to describe each type of main bonding pattern encountered and Hirshfeld surfaces to consider all secondary contacts, which, given their number, play a key role in the structure building and packing efficiency. Indeed, according to Desiraju,[34] the presence or absence of those weaker interactions could even be a determinant for the patterns formed by the stronger hydrogen bonds in the crystal.

Type I: p-OMe, o-Ph, m-F, p-F, m-Cl, p-Cl, m-Br, p-Br, m-NO_2, p-NO_2. Type I structures are characterized by repeating [R^2_2 (9)] ring motifs (Figure 2): the imine lone pair of a first molecule (A) accepts a H bond from an amide hydrogen of a second molecule (B), while the amide hydrogen of the first molecule donates a hydrogen bond to the carbonyl

DOI: 10.1021/acs.cgd.5b00621
Cryst. Growth Des. 2015, 15, 4005−4019

Table 1. Crystallographic Parameters of the 23 New Structures Sorted by Type

type I compounds	o-Ph	p-OMe	p-F	p-Cl	p-Br	p-NO2	m-F	m-Cl	m-Br	m-NO_2
structural formula	$C_{21}H_{18}N_2O$	$C_{16}H_{16}N_2O_2$	$C_{15}H_{13}N_2OF$	$C_{15}H_{13}N_2OCl$	$C_{15}H_{13}N_2OBr$	$C_{15}H_{13}N_3O_3$	$C_{15}H_{13}N_2OF$	$C_{15}H_{13}N_2OCl$	$C_{15}H_{13}N_2OBr$	$C_{15}H_{13}N_3O_3$
formula weight (g/mol)	314.37	268.31	256.27	272.72	317.17	283.28	256.27	272.72	317.17	283.28
space system	monoclinic	monoclinic	monoclinic	monoclinic	monoclinic	monoclinic	monoclinic	orthorhombic	orthorhombic	orthorhombic
space group	$P2_1$	$P2_1$	$P2_1$	$P2_1$	$P2_1$	$P2_1$	$P2_1$	$P2_12_12_1$	$P2_12_12_1$	$P2_12_12_1$
a (Å)	10.3943(8)	6.7394(3)	6.8172(8)	6.7343(4)	6.7098(4)	6.7108(4)	6.9740(3)	6.9705(3)	7.0276(4)	7.1806(6)
b (Å)	7.7222(5)	7.9886(3)	7.9216(9)	8.0362(4)	8.0495(4)	7.9363(4)	7.8282(3)	7.7622(4)	7.445(5)	7.7128(7)
c (Å)	11.8976(10)	13.3084(10)	12.594(2)	12.9186(7)	13.1003(8)	13.2410(8)	12.5581(6)	25.4745(12)	25.6078(13)	25.267(2)
α (deg)	90	90	90	90	90	90	90	90	90	90
β (deg)	112.922(10)	94.308(5)	103.040(16)	100.314(6)	98.867(6)	98.269(6)	105.511(5)	90	90	90
γ (deg)	90	90	90	90	90	90	90	90	90	90
V (Å^3)	879.574	714.478	662.577	687.834	699.098	697.87	660.625	1378.33	1393.71	1399.35
Z	2	2	2	2	2	2	2	4	4	4
R_1-factor (%)	3.48	5.05	4.27	3.07	4.46	3.97	3.03	3.5	3.6	4.22
d (g·cm^{-3})	1.187	1.247	1.285	1.317	1.507	1.348	1.288	1.314	1.512	1.345

type II compounds	m-Me	o-Me	o-Ome FI	o-F	o-Cl FI	o-Cl FII	o-Cl FIII	o-Br	o-NO_2
structural formula	$C_{16}H_{16}N_2O$	$C_{16}H_{16}N_2O$	$C_{16}H_{16}N_2O_2$	$C_{15}H_{13}N_2OF$	$C_{15}H_{13}N_2OCl$	$C_{15}H_{13}N_2OCl$	$C_{15}H_{13}N_2OCl$	$C_{15}H_{13}N_2OBr$	$C_{15}H_{13}N_3O_3$
formula weight (g/mol)	252.31	252.31	268.31	256.27	272.72	272.72	272.72	317.17	283.28
space system	orthorhombic	orthorhombic	orthorhombic	monoclinic	orthorhombic	orthorhombic	orthorhombic	orthorhombic	orthorhombic
space group	$P2_12_12_1$	$P2_12_12_1$	$P2_12_12_1$	$C2$	$Pna2_1$	$P2_12_12_1$	$P2_12_12_1$	$P2_12_12_1$	$P2_12_12_1$
a (Å)	5.1707(5)	5.2563(5)	5.1883(6)	20.3160(18)	18.549(3)	5.4131(2)	5.20340(10)	5.2600(3)	5.2320(4)
b (Å)	13.2714(12)	9.7698(12)	9.8853(10)	5.2050(3)	13.827(2)	13.2515(6)	9.7982(2)	9.7112(5)	13.7900(13)
c (Å)	20.434(2)	26.617(3)	27.403(3)	13.5364(14)	5.3162(7)	18.5144(9)	26.4764(5)	26.707(2)	18.6379(17)
α (deg)	90	90	90	90	90	90	90	90	90
β (deg)	90	90	90	114.387(12)	90	90	90	90	90
γ (deg)	90	90	90	90	90	90	90	90	90
V (Å^3)	1402.23	1366.86	1405.44	1303.69	1363.48	1328.07	1349.87	1364.22	1344.71
Z	4	4	4	4	4	4	4	4	4
R_1-factor (%)	4.74	6.53	4.51	3.51	4.48	3.58	3.17	3.79	5.09
d (g·cm^{-3})	1.195	1.226	1.268	1.306	1.329	1.364	1.342	1.554	1.399

type III compounds	p-Me	p-Ph	type IV compounds	m-OMe	type V compounds	o-OMe FII
structural formula	$C_{16}H_{16}N_2O$	$C_{21}H_{18}N_2O$	structural formula	$C_{16}H_{16}N_2O_2$	structural formula	$C_{16}H_{16}N_2O_2$
formula weight (g/mol)	252.31	314.37	formula weight (g/mol)	268.31	formula weight (g/mol)	268,31
space system	monoclinic	monoclinic	space system	monoclinic	space system	monoclinic
space group	$P2_1$	$P2_1$	space group	$P2_1$	space group	$C2/c$
a (Å)	8.2225(4)	8.3299(3)	a (Å)	8.6581(7)	a (Å)	25.096(2)
b (Å)	5.7932(3)	5.7214(2)	b (Å)	5.1375(3)	b (Å)	5.6957(4)
c (Å)	14.5687(6)	17.5391(5)	c (Å)	15.7993(10)	c (Å)	20.3318(15)
α (deg)	90	90	α (deg)	90	α (deg)	90
β (deg)	90.377(4)	91.143(3)	β (deg)	100.982(7)	β (deg)	107.199(6)
γ (deg)	90	90	γ (deg)	90	γ (deg)	90
V (Å^3)	639.959	835.724	V (Å^3)	689.899	V (Å^3)	2776.26
Z	2	2	Z	2	Z	8

DOI: 10.1021/acs.cgd.5b00621
Cryst. Growth Des. 2015, 15, 4005−4019

Table 1. continued

type III compounds	p-Me	p-Ph	type IV compounds	m-OMe	type V compounds	o-OMe FII
R_1-factor (%)	3.09	3.29	R_1-factor (%)	4.27	R_1-factor (%)	3.62
d (g·cm^{-3})	1.207	1.249	d (g·cm^{-3})	1.292	d (g·cm^{-3})	1.284

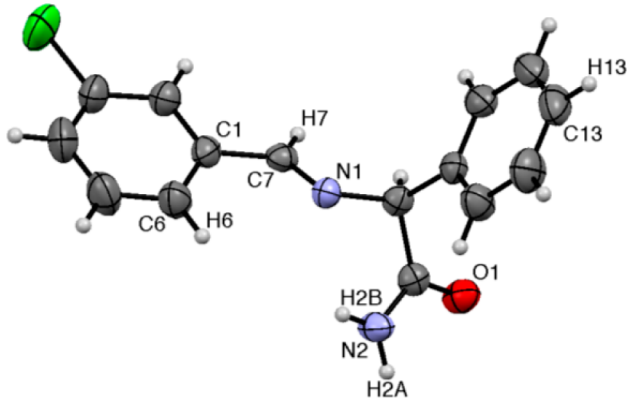

Figure 1. ORTEP plot (Mercury software 3.0) of m-Cl showing crystallographic numbering scheme on the atoms potentially involved in inter- and intramolecular interactions in the various structures.

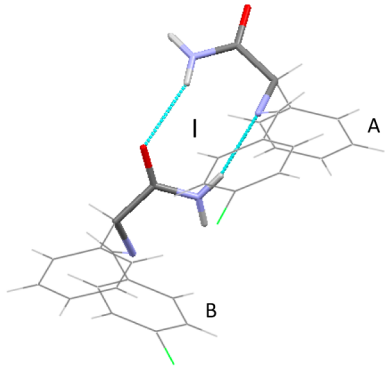

Figure 2. Type I motif displaying a [$R^2_2(9)$] ring between two molecules (A and B) of p-Cl.

of the second molecule. Each molecule is therefore involved in four different hydrogen bonds, with every potential H bond former being used.

Consecutive ring motifs produce zigzag ladders, containing two parallel infinite hydrogen-bond chains, described in graph set notation as [$C^2_2(7)$] and directed along the *b*-axis. From one sport of the ladder to the other, molecules are rotated by 180° around the *b*-axis; all phenyl groups point outward.

The one-dimensional ladders are stacked periodically along the *a* and *c* axes (Figure 3).

Type I structures crystallize either in the monoclinic $P2_1$ or in the orthorhombic $P2_12_12_1$ space groups.

Concerning the weaker hydrogen bonds, a particularly strong C−H···O interaction is found between C6—H6 and O1 (Figure 4 and Table 4). This is in accordance with the results of Lo Presti et al. (2006) stating that C--H···O bonds of comparable strength to O--H···O bonds can exist in organic molecules.[35]

One can also note the presence of a weaker C−H···O bond (C7−H7···O1) directed along the *a*-axis connecting the carbonyl of one ladder to the imine hydrogen H7 of another ladder and influencing the tridimensional arrangement. However, this additional interaction does not occur in o-Ph because the biphenyl group prevents a sufficient proximity between adjacent ladders, the packing stability being due supposedly to hydrophobic interactions in this case (see below). This interladder interaction is not present either in m-NO_2, which rather shows a C5−H5···O3 bond, involving the nitro group holding ladders together (Figure 5).

DOI: 10.1021/acs.cgd.5b00621
Cryst. Growth Des. 2015, 15, 4005−4019

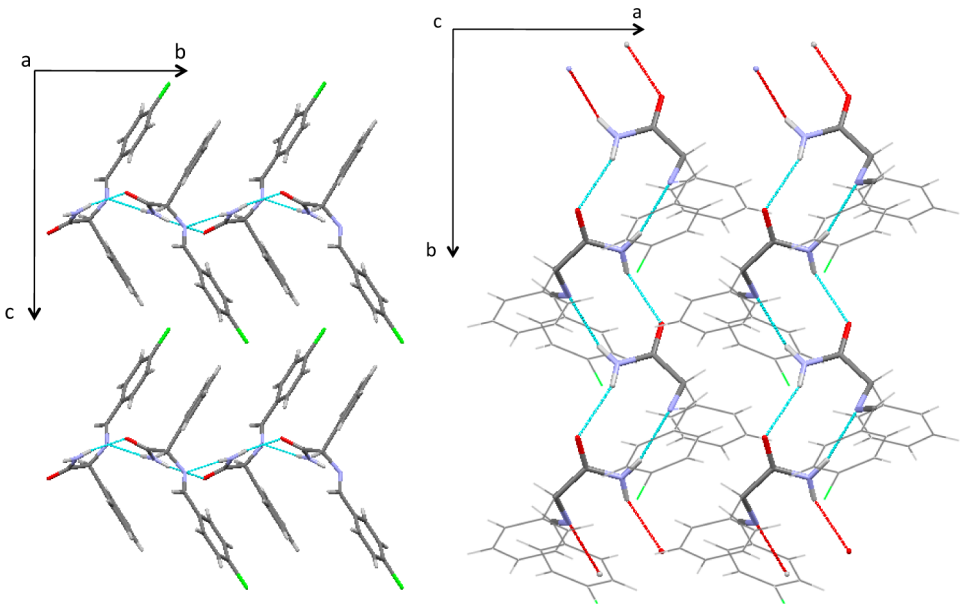

Figure 3. Stacking of p-Cl in the *bc* (left) and *ab* (right) planes, displaying zigzag ladders with $[C^2_2(7)]$ graph set notation, forming undulating one-dimensional ribbons.

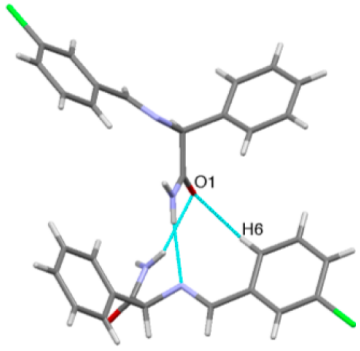

Figure 4. C6—H6···O1 intermolecular bond in type I structures (m-Cl).

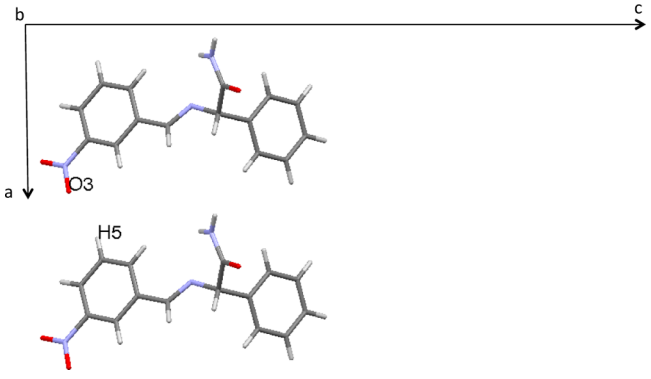

Figure 5. C5—H5···O3 bond in m-NO_2.

In addition, comparison of $\pi-\pi$ stacking, C—H···π and other hydrophobic interactions in the different structures can easily be performed by analyzing the 2D fingerprint plot and the corresponding Hirshfeld surfaces of the molecules in the different structures. Indeed, they give us a complete view of intermolecular interactions, focusing not solely on "assumed important interactions".[26]

Among type I structures, disparities are found within the secondary interactions.

For example, the 2D plot of m-F (Figure 6, left and middle) displays so-called "horns" between the spikes, while other meta-substituted type I structures do not. Those account for the presence of the short C—F···H interaction present in m-F.

In addition, comparing it with the 2D fingerprint plot of m-Br (Figure 6, right), one observes that the latter structure is less efficiently packed, as illustrated by the presence of a diffuse blue region at high distances.

Similarly, the 2D fingerprint plot of o-Ph differs significantly from the others by the presence of a bump between the spikes and of a pair of wings on the other side of the spikes (Figure 7). The central bump corresponds to all the hydrophobic H···H contacts, while the external wings represent the C—H···π interactions which are highly represented in this particular structure, visible as orange zones above the rings on the de Hirshfeld surface (Figure 8).

Type II: m-Me, o-Me, o-OMe FI, o-F, o-Cl (FI, FII, FIII), o-Br, o-NO_2. As for type I structures, type II structures are also organized in ladders but this time running along the *a*-axis. The ladders are constituted by the succession of inverted $[R^2_3(8)]$ ring motifs involving three molecules (two adjacent ones, A and C, and one on the other side of the ladder, B). The carbonyl of the first molecule (A) forms a bifurcated H bond with one amide hydrogen of the second (B) and the third (C) molecule. In addition, the second amide hydrogen of the third molecule is linked to the carbonyl of the second molecule (Figure 9).

As for type I structures, each molecule takes part in four H bonds, but this time two donating hydrogen bonds using the amide hydrogens and two accepting bonds through the carbonyl group. Contrary to the type I structures, the imine is not included in any H bonding pattern in type II structures.

Contrary to type I, no distinctive interladder interaction is reported. However, when the substituent is a halogen/nitro group, an extra intramolecular hydrogen bond is formed between the substituent and the imine hydrogen H7.

The successive ring motifs form two parallel hydrogen-bonded infinite chains C(4) directed along the *a*-axis (Figure

DOI: 10.1021/acs.cgd.5b00621
Cryst. Growth Des. 2015, 15, 4005−4019

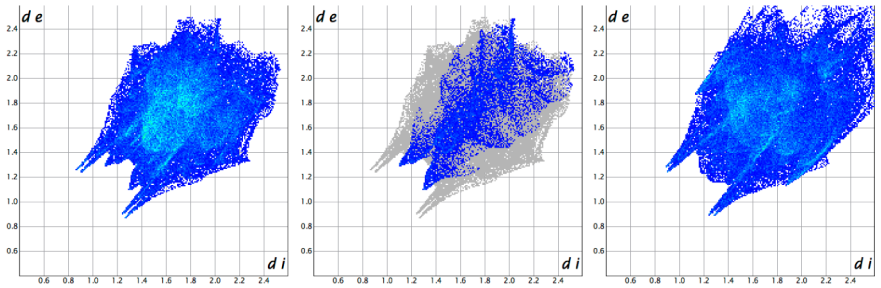

Figure 6. 2D fingerprint plots of m-F (left and central figure) displaying the "horns" corresponding to the short C−H···F interaction (highlighted on the central figure). On the right, the 2D fingerprint plots of m-Br with no horns and less efficient packing.

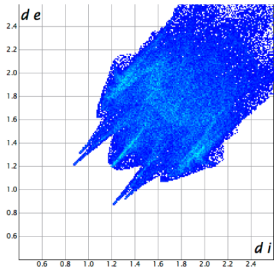

Figure 7. 2D fingerprint plot of o-Ph displaying a central bump, corresponding to H···H contacts, and a pair of external wings corresponding to the C−H···π interactions.

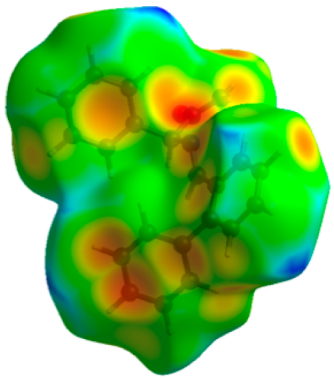

Figure 8. Hirshfeld surface of o-Ph mapped with d_e and displaying bright orange regions above the rings, corresponding to various C−H···π interactions.

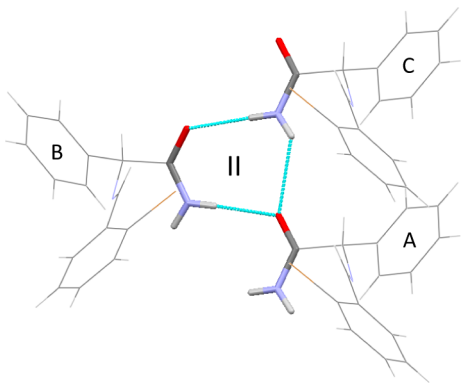

Figure 9. Type II motif displaying a $[R^2_3(8)]$ ring formed by three molecules (A, B and C) of o-Br.

10). Ladders are almost planar, except in o-F structure, in which ladders are slightly undulating.

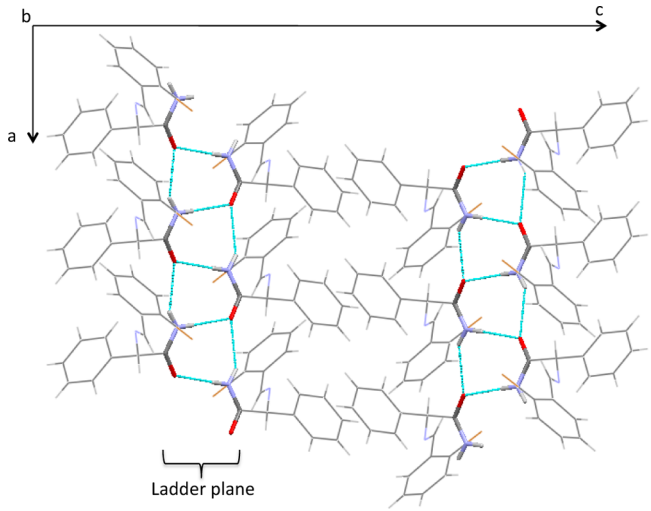

Figure 10. o-Br stacking in the *ac* plane, displaying infinite chains C(4) creating almost planar ladders.

Although all motif II structures display the same hydrogen bonding patterns, their overall molecular packing is less homogeneous. Therefore, the type II structures can be sorted in three different subgroups according to the stacking of the ladders along the *b* and *c* axes.

A first subgroup includes structures m-Me, o-Cl (FI, FII), and o-NO_2. Ladders are stacked in alternating rows along the *c*-axis (Figure 11), except for o-Cl FI, in which rows alternate along the *a*-axis. The ladders planes are parallel within a row but form an angle with ladders planes situated in the next row. On top, consecutive ladders rows are interpenetrating (Figure 11).

In the second subgroup (o-Me, o-OMe FI, o-Cl FIII, and o-Br), one observes the same packing as in the first subgroup, except that subsequent rows do not interpenetrate, but form herringbone arrangements (Figure 12).

This is because the inclination angle of the ladders planes with respect to the *b*-axis is more pronounced in this last subgroup (Figure 13).

In the last subgroup (o-F), ladders planes are parallel within and between rows (Figure 14). This is therefore the only compound that crystallizes in the monoclinic space group *C*2; all the other compounds in type II belong to orthorhombic space groups.

The analysis of the secondary interactions also reveals disparities among type II structures. For most ortho substituted type II structures, there is a spike on the diagonal of the 2D fingerprint plot. This accounts for the directional H···H interactions found in those structures. Those interactions are

DOI: 10.1021/acs.cgd.5b00621
Cryst. Growth Des. 2015, 15, 4005−4019

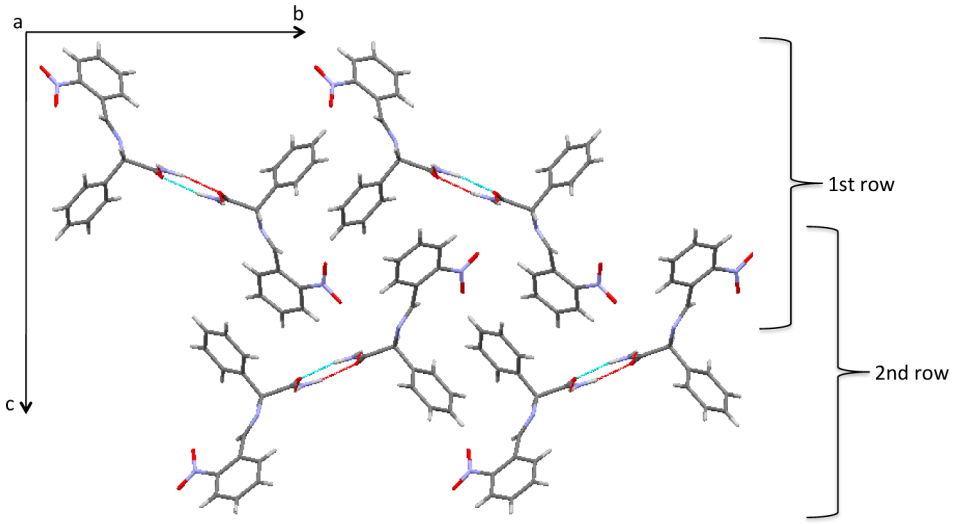

Figure 11. o-NO_2 rows stacking in the *bc* plane.

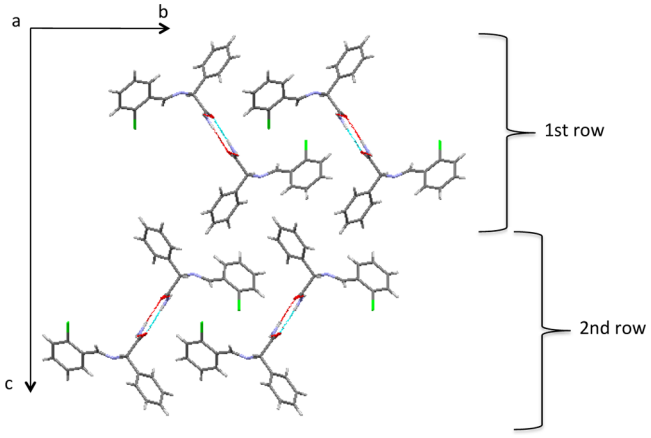

Figure 12. o-Cl (FIII) stacking in the *bc* plane exhibiting herringbone arrangement.

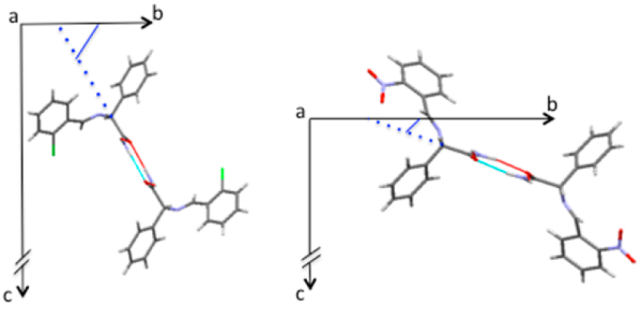

Figure 13. Inclination angle of the ladders planes in the *bc* plane with respect to the *b*-axis is smaller in the first subgroup (right, o-NO_2) than in the second (left, o-Cl (FIII)).

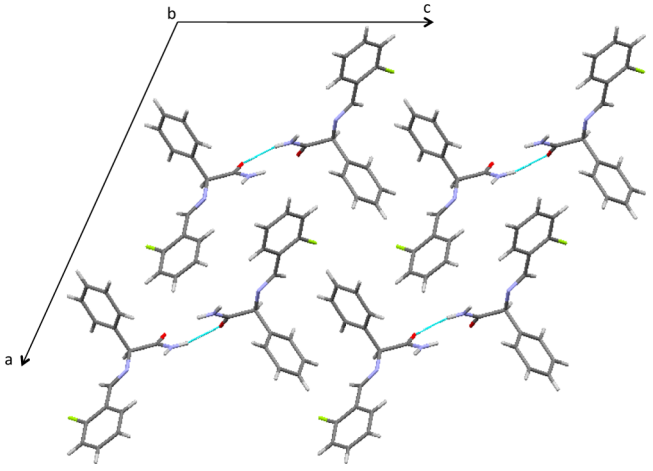

Figure 14. o-F stacking in the *ac* plane.

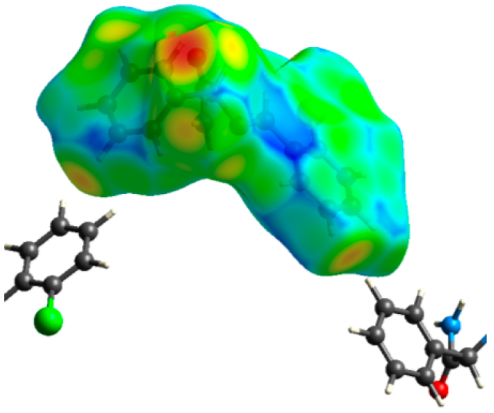

Figure 15. Hirshfeld surface of o-Cl (FII) mapped with d_e function. Directional H···H contacts are represented.

depicted by orange areas on the bottom left and right of the Hirshfled surface of o-Cl FII, together with the interacting molecules (Figure 15). The strength of those interactions varies tremendously according to the nature of the substituent as well as the nature of the polymorph as shown by the three o-Cl structures (Figure 16).

Type III: p-Me and p-Ph. These structures are characterized by head-to-tail catemers, propagating along the *b*-axis and characterized by a $[C^2_2(8)]$ infinite hydrogen-bonded chain motif: a H bond connects the carbonyl of a molecule to one amide hydrogen of a second molecule, related to the first one by the 2-fold screw axis in $P2_1$ (Figure 17). The imine does not participate in any supramolecular motif, and only one hydrogen on the amide nitrogen atom is involved in H bond formation.

DOI: 10.1021/acs.cgd.5b00621
Cryst. Growth Des. 2015, 15, 4005−4019

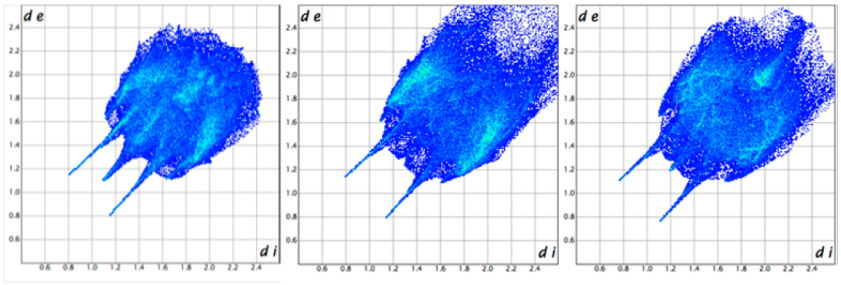

Figure 16. 2D fingerprint plot of o-Cl FII (left), FI (middle) and FIII (right).

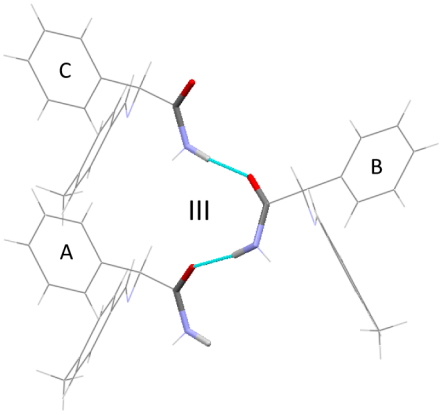

Figure 17. Type III motif displaying $[C^2_2(8)]$ hydrogen-bonded infinite chains formed by three molecules (A, B, and C) of p-Me.

Hence, unlike type I and II structures, only two hydrogen bonds are formed per molecule in this type.

Type III structures exhibit an interchain link joining the carbonyl and the para hydrogen on the phenyl group, providing chain cohesion along the *a*-axis (Figure 18). The same connection is present in type IV albeit with greater strength (see Table 4 below).

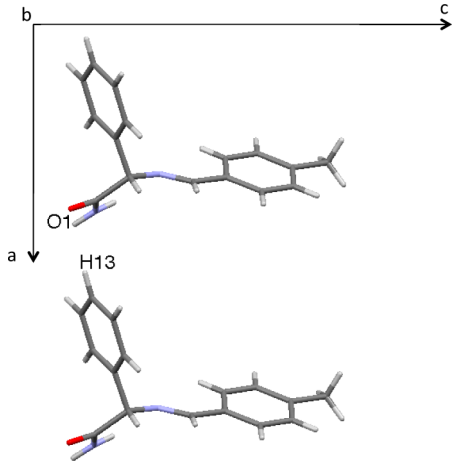

Figure 18. C13—H13···O1 bond in p-Me.

Besides, an additional C8—H8···O1 interaction is present in p-Ph (but not in p-Me). Accordingly, the catemer formed by p-Me molecules is planar (Figure 17), while it is angular (113° between successive hydrogen bonds in the catemer) in the p-Ph structure (Figure 19).

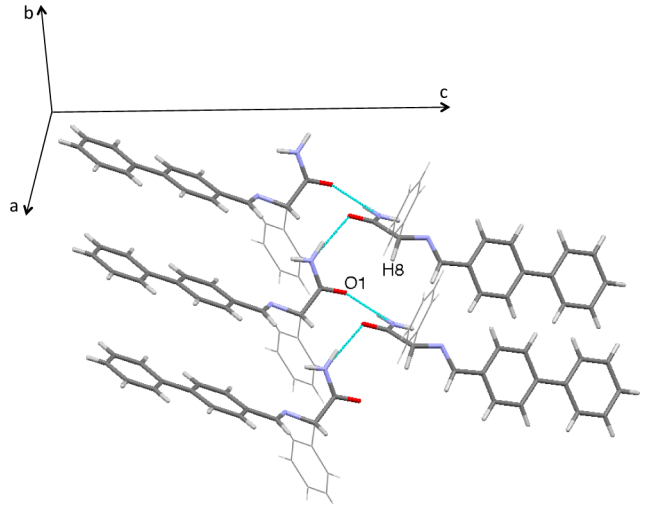

Figure 19. C8—H8···O1 intermolecular interaction and angular catemer in p-Ph (type III).

The network can be described by the stacking of non-interacting chains along the *a* and *c* axes. As in o-F (type II), chains are intercalated and chains planes parallel within and between rows in the *bc* plane (Figure 20).

Both p-Me and p-Ph structures belong to the monoclinic space group $P2_1$.

As for the other types, the two type III structures differ significantly from one another with respect to the hydrophobic contacts. The p-Me 2D fingerprint plot is characterized by a central bump and external wings, corresponding to the presence of H···H contacts and C—H···π interactions respectively, while p-Ph does not have any of these features (Figure 21).

Type IV: m-OMe. This type of structures exhibit succession of $[R^3_3(11)]$ ring motifs involving three molecules (Figure 22). A H bond joins one amide hydrogen of a first molecule (A) to the imine of a second molecule (C). Another H bond links the second molecule carbonyl to the third molecule's amide hydrogen (B). A last H bond exists between the third molecule's carbonyl (B) and the first molecule's amide hydrogen (A).

Those successive motifs form one inner $[C^2_2(8)]$ and two outer C(5) hydrogen-bonded infinite chains directed along the *b*-axis (Figure 23).

Contrary to the type II structures, the imine takes part in the hydrogen bonding patterns, and each carbonyl accepts only one H bond. Furthermore, unlike the type III structures, both amide hydrogens are involved in such interactions. Thus, as in type I, each molecule is involved in four different hydrogen bonds.

DOI: 10.1021/acs.cgd.5b00621
Cryst. Growth Des. 2015, 15, 4005−4019

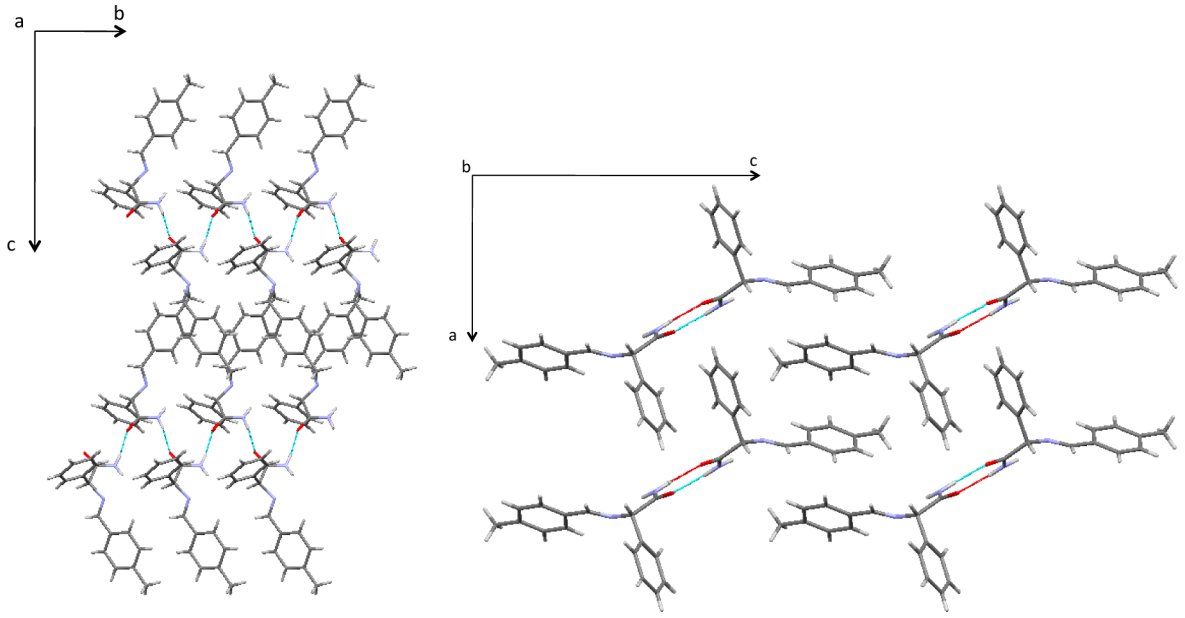

Figure 20. p-Me stacking in *bc* and *ac* planes.

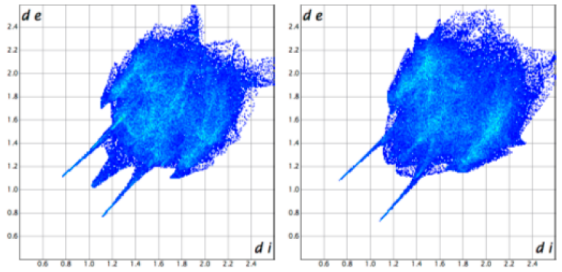

Figure 21. 2D fingerprint plot of p-Me (left) and p-Ph (right). p-Me plot displays a central bump and a pair of external wings corresponding to H···H contacts and C−H···π interactions, respectively.

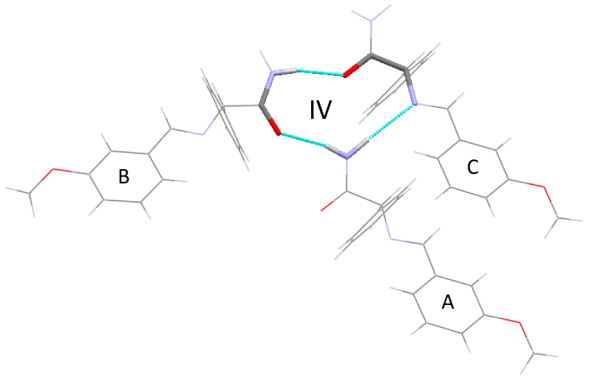

Figure 22. Type IV motif displaying a $[R^3_3(11)]$ ring formed by three molecules (A, B, and C) of m-OMe.

Those motifs generate one-dimensional hydrogen bonded twisted ladders stacked along the *a* and *c* directions. Once again, those twisted ladders are intercalated, and ladders planes are parallel within and between rows in the *ac* plane (Figure 24).

Concerning other interactions, one can denote the presence of particularly strong C13—H13···O1 (Figure 25 and Table 4) interactions.

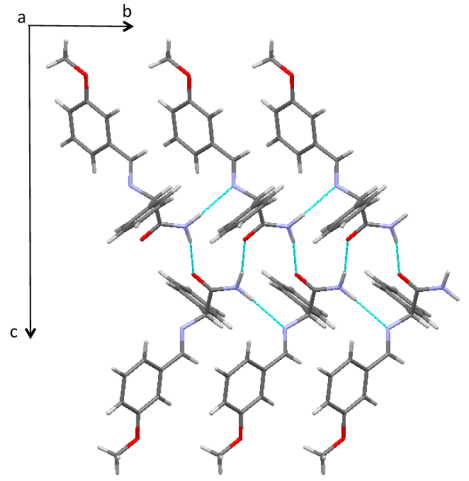

Figure 23. Inner $[C^2_2(8)]$ and outer C(5) hydrogen-bonded infinite chains constituted by successive motifs.

The type IV structure also crystallizes in the monoclinic space-group $P2_1$.

On the 2D fingerprint plot of type IV, the only significant feature concerning the hydrophobic contacts is the presence of horns near the diagonal, which are because in the $[R^3_3(11)]$ hydrogen bonding pattern of this structure, the amide hydrogens of two interacting molecules are very close and hence provide a nondirectional H···H contact (Figure 26).

Type V: o-OMe FII. The type V structure has a dimer motif as the main pattern. The dimers are formed by amide−amide homosynthons $[R^2_2(8)]$ joining the amides of two molecules (A and B, Figure 27). It is the only type in which no infinite motifs (i.e., chains) are present. As in types II and III, the imine lone pair does not take part in any intermolecular hydrogen bonding and as in type III, only one amide hydrogen gives a hydrogen bond. Hence, as in type III, each molecule forms only two distinct intermolecular hydrogen bonds. However, a weak intramolecular hydrogen bond is formed between the imine hydrogen H7 and the oxygen O2 on the substituent.

DOI: 10.1021/acs.cgd.5b00621
Cryst. Growth Des. 2015, 15, 4005−4019

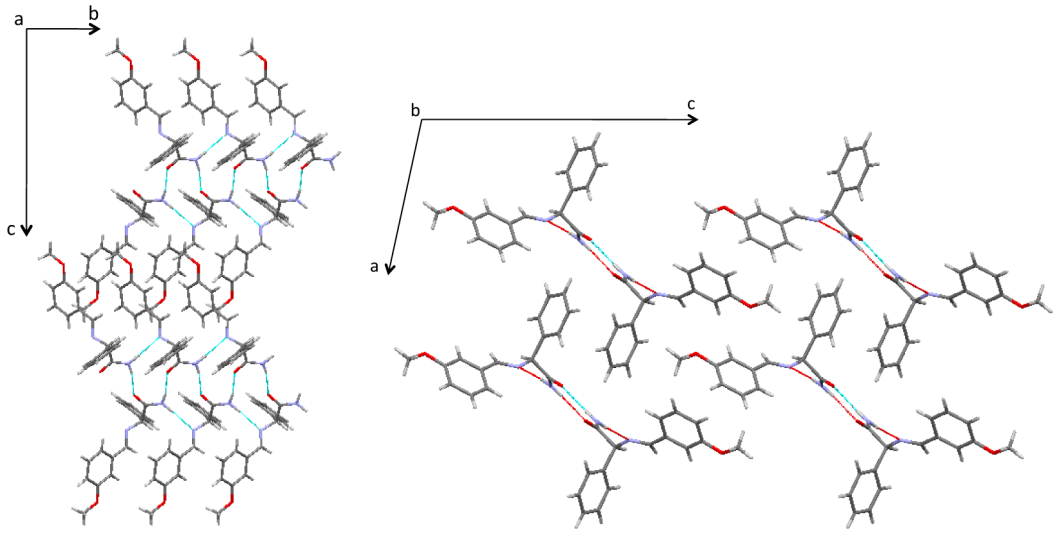

Figure 24. Stacking of m-OMe in the *bc* and *ac* planes exhibiting one-dimensional hydrogen bonded tapes.

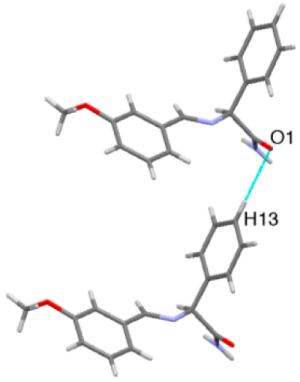

Figure 25. C13—H13···O1 interchain bond in type IV structure (m-OMe).

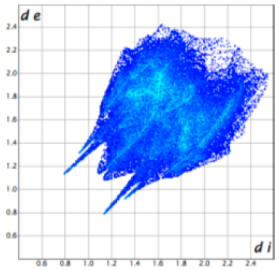

Figure 26. 2D fingerprint plot of m-OMe displaying a pair of horns near the diagonal, corresponding to close nondirectional H···H contact in the hydrogen bonding pattern.

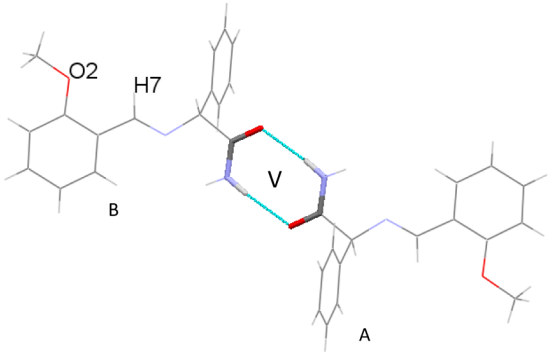

Figure 27. Type V motif displaying a $[R^2_2(8)]$ ring formed by two molecules (A and B) of o-OMe.

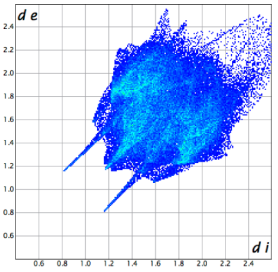

Figure 28. 2D fingerprint plot of o-OMe displaying a central bump and a diffuse region at the high distances.

Overall, the packing is as in type II first subgroup: dimers are stacked in alternating and intercalated rows along the *c*-axis.

Type V structure belongs to the monoclinic space group *C*2/*c*.

As main feature, the 2D fingerprint of type V structure shows a central bump corresponding to the hydrophobic H···H contacts. Furthermore, the structure seems to be less tightly packed according to the presence of a sparse region at the high distances on Figure 28.

DISCUSSION

The allocation of structures in different types (displayed in Table 2) reveals that

- All halogen/nitro meta/para substituted compounds show type I structures.
- All halogen/nitro ortho substituted compounds show type II structures.
- Structures with an alkyl/methoxy substituent are encountered in various types.
- Type I and II motifs are by far the most frequently encountered, with 19 out of the 23 structures belonging to these types.

DOI: 10.1021/acs.cgd.5b00621
Cryst. Growth Des. 2015, 15, 4005−4019

Table 2. Graph Sets and Bond Nature of the Most Prominent Features in Each Type, along with All Structures Belonging to Those Types

type	compounds	hydrogen bonding patterns	main interactions[a]	interactions localization
I	o-Ph, p-OMe, p-F, p-Cl, p-Br, m-F, P-NO_2, m-Cl, m-Br, m-NO_2	$[R^2_2(9)]$, $[C^2_2(7)]$	N2--H2A···N1	intermolecular
			N2--H2B···O1	intermolecular
			N2--H2B···N1	intramolecular
II	m-Me, o-Me, o-Ome FI, o-F, o-Cl, o-Br, o-NO_2	$[R^2_3(8)]$, C(4)	N2--H2A···O1	intermolecular
			N2--H2B···O1	intermolecular
			N2--H2B···N1	intramolecular
III	p-Me, p-Ph	C(8)	N2--H2A···O1	intermolecular
			N2--H2B···N1	intramolecular
IV	m-OMe	$[R^3_3(11)]$, $[C^2_2(7)]$, C(5)	N2--H2B···N1	intermolecular
			N2--H2A···O1	intermolecular
			N2--H2B···O1	intermolecular
V	o-OMe FII	$[R^2_2(8)]$	N2--H2A···O1	intermolecular
			N2--H2B···N1	intramolecular

[a]C---H···O interactions not taken into account.

This leads to the question of whether the attribution to a given type is mostly due to electronic or rather steric effects specific to the substituents or their position on the benzylidene.

Concerning the electronic effects, we note that both meta and para halogen substituted moieties exhibit type I structures. However, theoretical charges generated by mesomeric and inductive effects of halogens are located at different positions on the benzylidene for meta- and para-substituted compounds. In other words, these charges do not impact the formation of hydrogen bonds involving the benzylidene hydrogens or the imine nitrogen. This result is in agreement with density functional theory (DFT) calculations, showing the charges present on the benzylidene atoms are very similar regardless of the nature and position of the substituent on the ring. One can thus conclude that mesomeric and inductive factors of halogens do not significantly affect the structural outcome and that their position (and subsequent steric occupation) on the ring may play a more important role.

Since $\pi-\pi$ stacking, C−H···π and other hydrophobic interactions vary tremendously within a type of structures, they should not be determining for type affiliation either, and the discussion below will therefore focus on the stronger interactions present in the various structures (Table 3). Their analysis reveals that only four different main interactions occur, no matter the overall hydrogen motifs formed. Indeed, there are two potential strong donors (both amide hydrogens) and two potential strong acceptors (the imine nitrogen and the carbonyl oxygen) common to all compounds, so the combinations are limited.

Among those interactions, the N2--H2···N1 bond is present in each type, following Etter's rule of the best H-bond acceptor and donor associating with each other.[36] In types II, III and V, this interaction is intramolecular while being intermolecular in type IV. In type I, an intramolecular N2--H2B···N1 is found in addition to an intermolecular N2--H2A···N1.

However, comparing the intermolecular bonds lengths and angles, it appears that N2--H2···O1, which is also present in every type, is the shortest and more linear interaction. In fact, the lone pair of the imine nitrogen is more basic than the carbonyl oxygen but also more sterically hindered (by the phenyl groups situated on both sides). The carbonyl oxygen is thus more accessible and prompt to form short hydrogen bonds with neighboring molecules.

Furthermore, according to Galek et al.,[37] structures where all the good donors are satisfied (i.e., forming their preferential number of coordination) are favored, even if some acceptors are left unemployed. This is in accordance with our results: in every structure type, both amide hydrogens take part in H bonds, while for some types, the imine accepts no hydrogen bond. Similarly, the carbonyl can accept two hydrogen bonds, but this happens only in type II structures. In the other types, the carbonyl does not form bifurcated hydrogen bonds.

However, depending on the type, H2B forms an intra- or an intermolecular bond. This latter is notably stronger than the former, as the corresponding bond lengths and angles testify.

Moreover, as Bilton emphasizes,[38] the most probable intramolecular H-bonding motifs are planar conjugated six-membered rings. Hence, in structures where they are observable, certain six-membered ring motifs are almost 100% likely to form.[39] Yet the present intramolecular H-bond (N2--H2B··N1) rather forms a five-membred ring without π-electron delocalization. It has thus a reduced probability to appear in a given structure.

This is supported by the fact that, usually, when a donor hydrogen is involved in a intramolecular H bond, it is less likely to participate in an additional intermolecular contact.[38] Yet, in types I and II, H2B forms an intra- and an intermolecular H bond. This proves that this particular intramolecular bond is so weak that it does not prevent additional interactions.

Given that, one can even question if the intramolecular (N2--H2B··N1) bond identified by Platon software[40] is really a true hydrogen bond or rather an "artifact of other stronger interactions" as Taylor called them.[41] This is supported by Wood et al. analysis, showing that contacts with D−H···A angles below 120° are not significant interactions *per se*.[42]

In an attempt to classify the different types according to their respective stability, we notice that type III and V structures display only one strong hydrogen bond (angle >120°), while the other types possess two, and that H2B is involved only in the aforementioned very weak intramolecular bond. Hence those two types structures are less stable than the other types structures, explaining why they are among the less encountered. Accordingly, among the two polymorphs identified for o-OMe structure, form I is expected to be the thermodynamically stable one.

In the three other types (I, II, and IV) structures, the two strong hydrogen bonds formed seem to be of comparable

DOI: 10.1021/acs.cgd.5b00621
Cryst. Growth Des. 2015, 15, 4005−4019

Table 3. Bond Lengths (Angstrom) and Angles (deg) of the Main Intermolecular Hydrogen Bonds in the 20 Compounds Sorted by Types

type I compounds	D−H···A	linked molecules	D−H (Å)	H···A (Å)	D···A (Å)	D−H···A (Å)	symmetry
o-Ph	N2−H2A···N1	B−A	0.92(2)	2.32(2)	3.203(2)	161(2)	1−*x*,−1/2+*y*,1−*z*
	N2−H2B···O1	A−B	0.95(3)	2.14(3)	2.998(2)	150.2(19)	1−*x*,1/2+*y*,1−*z*
	N2−H2B···N1	intramolecular	0.95(3)	2.34(2)	2.736(2)	104.5(16)	
p-OMe	N2−H2A···N1	B−A	0.86(3)	2.28(3)	3.099(3)	159(2)	2−*x*,−1/2+*y*,1−*z*
	N2−H2B···O1	A−B	0.86(3)	2.30(3)	3.088(3)	153(2)	2−*x*,1/2+*y*,1−*z*
	N2−H2B···N1	intramolecular	0.86(3)	2.33(3)	2.692(3)	105(2)	
m-F	N2−H2A···N1	B−A	0.85(2)	2.28(2)	3.1064(19)	164(2)	1−*x*,−1/2+*y*,1−*z*
	N2−H2B···O1	A−B	0.85(2)	2.29(2)	3.0808(18)	154.9(14)	1−*x*,1/2+*y*,1−*z*
	N2−H2B···N1	intramolecular	0.85(2)	2.343(16)	2.6919(19)	105.0(12)	
p-F	N2−H2A···N1	B−A	0.86	2.28	3.103(3)	161	−*x*,−1/2+*y*,−*z*
	N2−H2B···O1	A−B	0.86	2.26	3.064(3)	156	−*x*,1/2+*y*,−*z*
	N2−H2B···N1	intramolecular	0.86	2.34	2.702(3)	106	
m-Cl	N2−H2A···N1	B−A	0.88(2)	2.24(2)	3.107(2)	169.2(19)	1−*x*,1/2+*y*,1/2−*z*
	N2−H2B···O1	A−B	0.84(2)	2.32(2)	3.087(2)	153(2)	1−*x*,−1/2+*y*,1/2−*z*
	N2−H2B···N1	intramolecular	0.84(2)	2.33(2)	2.691(2)	106.4(17)	
p-Cl	N2−H2A···N1	B−A	0.90(2)	2.26(2)	3.146(2)	165.0(19)	1−*x*,−1/2+*y*,1−*z*
	N2−H2B···O1	A−B	0.86(2)	2.27(2)	3.069(2)	154.8(18)	1−*x*,1/2+*y*,1−*z*
	N2−H2B···N1	intramolecular	0.86(2)	2.33(2)	2.700(2)	106.3(16)	
m-Br	N2−H2A···N1	B−A	0.89	2.28	3.115(3)	156	−*x*,−1/2+*y*,3/2−*z*
	N2−H2B···O1	A−B	0.93	2.21	3.089(3)	157	−*x*,1/2+*y*,3/2−*z*
	N2−H2B···N1	intramolecular	0.9300	2.34	2.680(3)	101	
p-Br	N2−H2A···N1	B−A	0.84(7)	2.32(8)	3.139(7)	167(6)	−*x*,−1/2+*y*,1−*z*
	N2−H2B···O1	A−B	0.87(7)	2.26(7)	3.083(6)	159(4)	−*x*,1/2+*y*,1−*z*
	N2−H2B···N1	intramolecular	0.87(7)	2.36(5)	2.700(6)	103(4)	
m-NO_2	N2−H2A···N1	B−A	0.87(2)	2.29(2)	3.134(3)	164(2)	1−*x*,1/2+*y*,3/2−*z*
	N2−H2B···O1	A−B	0.85(3)	2.34(3)	3.090(3)	147.8(19)	1−*x*,−1/2+*y*,3/2−*z*
	N2−H2B···N1	intramolecular	0.85(3)	2.27(2)	2.687(3)	110.5(17)	
p-NO_2	N2−H2A···N1	B−A	0.91(3)	2.26(2)	3.127(2)	160(2)	2−*x*,−1/2+*y*,−*z*
	N2−H2B···O1	A−B	0.90(2)	2.21(2)	3.048(2)	154.0(18)	2−*x*,1/2+*y*,−*z*
	N2−H2B···N1	intramolecular	0.90(2)	2.33(2)	2.694(2)	104.2(15)	
type II compounds	D−H···A	linked molecules	D−H (Å)	H···A (Å)	D···A (Å)	D−H···A (Å)	symmetry
m-Me	N2−H2A··· O1	C−B/B−A	0.81(3)	2.15(3)	2.944(3)	169(3)	−1/2+*x*,−1/2−*y*,2−*z*
	N2−H2B···O1	C−A	0.92(3)	2.19(3)	2.962(3)	142(2)	−1+*x*,*y*,*z*
	N2−H2B···N1	intramolecular	0.92(3)	2.33(3)	2.726(3)	106(2)	
o-Me	N2−H2A···O1	C−B/B−A	0.93(3)	1.97(3)	2.889(3)	175(2)	−1/2+*x*,−1/2−*y*,1−*z*
	N2−H2B···O1	C−A	0.84(3)	2.50(3)	3.058(3)	124(2)	−1+*x*,*y*,*z*
	N2−H2B···N1	intramolecular	0.84(3)	2.36(3)	2.736(4)	108(2)	
o-OMe FI	N2−H2A···O1	C−B/B−A	0.94(2)	1.98(2)	2.915(3)	174(2)	1/2+*x*,−1/2−*y*,2−*z*
	N2−H2B···O1	C−A	0.82(3)	2.39(3)	2.978(3)	130(2)	1+*x*,*y*,*z*
	N2−H2B···N1	intramolecular	0.82(3)	2.40(3)	2.742(3)	107(2)	
o-F	N2−H2A···O1	C−B/B−A	0.86	2.14	2.959(2)	160	1/2−*x*,−1/2+*y*,1−*z*
	N2−H2B···O1	C-A	0.86	2.58	3.180(3)	128	*x*,−1+*y*,*z*
	N2−H2B···N1	intramolecular	0.86	2.34	2.705(2)	106	
o-Cl FI	N2−H2A···O1	C−B/B−A	0.86	2.08	2.934(4)	170	1−*x*,−*y*,−1/2+*z*
	N2−H2B···O1	C−A	0.86	2.43	3.107(5)	136	*x*,*y*,−1+*z*
	N2−H2B···N1	intramolecular	0.86	2.35	2.705(4)	105	
o-Cl FII	N2−H2A···O1	C−B/B−A	0.89(4)	2.08(4)	2.942(3)	165(3)	−1/2+*x*,1/2−*y*,2−*z*
	N2−H2B···O1	C−A	0.83(3)	2.58(3)	3.233(3)	138(3)	−1+*x*,*y*,*z*
	N2−H2B···N1	intramolecular	0.83(3)	2.33(3)	2.714(3)	109(2)	
o-Cl FIII	N2−H2A···O1	C−B/B−A	0.84(2)	2.04(2)	2.8819(19)	179(2)	1/2+*x*,3/2−*y*,2−*z*
	N2−H2B···O1	C−A	0.81(2)	2.45(3)	3.0248(19)	128.1(19)	1+*x*,*y*,*z*
	N2−H2B···N1	intramolecular	0.81(2)	2.43(2)	2.748(2)	104.3(19)	
o-Br	N2−H2A···O1	C−B/B−A	0.86	2.04	2.892(4)	172	1/2+*x*,3/2−*y*,−*z*
	N2−H2B···O1	C−A	0.86	2.51	3.074(4)	124	1+*x*,*y*,*z*
	N2−H2B···N1	intramolecular	0.86	2.37	2.743(4)	107	
o-NO_2	N2−H2A···O1	C−B/B−A	0.93(4)	1.97(4)	2.887(3)	168(3)	1/2+*x*,3/2−*y*,1−*z*
	N2−H2B···O1	C−A	0.91(4)	2.31(4)	3.015(3)	134(3)	1+*x*,*y*,*z*
	N2−H2B···N1	intramolecular	0.91(4)	2.38(4)	2.737(3)	104(3)	

DOI: 10.1021/acs.cgd.5b00621
Cryst. Growth Des. 2015, 15, 4005−4019

Table 3. continued

type III compounds	D−H···A	linked molecules	D−H (Å)	H···A (Å)	D···A (Å)	D−H···A (Å)	symmetry
p-Me	N2−H2A···O1	C−B/B−A	0.94(2)	1.96(2)	2.886(2)	172(2)	1−*x*,1/2+*y*,2−*z*
	N2−H2B···N1	intramolecular	0.86(2)	2.27(2)	2.704(2)	111.6(18)	
p-Ph	N2−H2A···O1	C−B/B-A	0.95(3)	1.88(3)	2.803(2)	164(2)	1−*x*,1/2+*y*,−*z*
	N2−H2B···N1	intramolecular	0.90(2)	2.20(3)	2.646(2)	110(2)	
type IV compounds	D−H···A	linked molecules	D−H (Å)	H···A (Å)	D···A (Å)	D−H···A (Å)	symmetry
m-OMe	N2−H2B···N1	A−C	0.98(3)	2.26(3)	3.241(3)	176(2)	*x*,1+*y*,*z*
	N2−H2A···O1	A−B/B−C	0.89(3)	2.04(3)	2.920(3)	167(3)	1−*x*,1/2+*y*,2−*z*
	N2−H2B···O1	A−C	0.98(3)	2.55(3)	3.054(3)	111.6(19)	*x*,1+*y*,*z*
type V compounds	D−H···A	linked molecules	D−H (Å)	H···A (Å)	D···A (Å)	D−H···A (Å)	symmetry
o-OMe FII	N2−H2A···O1	A−B/B−A	0.883(19)	2.099(19)	2.9773(17)	172.7(16)	−*x*,2−*y*,−*z*
	N2−H2B···N1	intramolecular	0.877(17)	2.276(18)	2.6881(17)	108.7(14)	

Table 4. Bond Lengths (Angstrom) and Angles (deg) of the C−H···O Intermolecular Interactions in Compounds of type I, III, and IV

type I compounds	D−H···A	linked molecules	D−H (Å)	H···A (Å)	D···A (Å)	D−H···A (Å)	symmetry
o-Ph	C6--H6···O1	A−B	0.93	2.54	3.466(2)	173	1−*x*,1/2+*y*,1−*z*
p-OMe	C6--H6···O1	A−B	0.93	2.43	3.357(3)	175	2−*x*,1/2+*y*,1−*z*
p-F	C6--H6···O1	A−B	0.93	2.49	3.415(3)	172	−*x*,1/2+*y*,−*z*
p-Cl	C6--H6···O1	A−B	0.93	2.47	3.396(2)	174	1−*x*,1/2+*y*,1−*z*
p-Br	C6--H6···O1	A−B	0.93	2.46	3.382(6)	173	−*x*,1/2+*y*,1−*z*
P-NO_2	C6--H6···O1	A−B	0.93	2.45	3.373(2)	171	2−*x*,1/2+*y*,−*z*
m-F	C6--H6···O1	A−B	0.93	2.56	3.470(2)	167	1−*x*,1/2+*y*,1−*z*
m-Cl	C6--H6···O1	A−B	0.93	2.49	3.414(2)	173	1−*x*,−1/2+*y*,1/2−*z*
m-Br	C6--H6···O1	A−B	0.93	2.48	3.403(4)	174	−*x*,1/2+*y*,3/2−*z*
m-NO_2	C6--H6···O1	A−B	0.93	2.54	3.468(3)	174	1−*x*,−1/2+*y*,3/2−*z*
type III compounds	D−H···A	linked molecules	D−H (Å)	H···A (Å)	D···A (Å)	D−H···A (Å)	symmetry
p-Ph	C8--H8···O1	A−B/B−C	1.00(2)	2.58(2)	3.396(2)	139.1(16)	1−*x*,−1/2+*y*,−*z*
type IV compounds	D−H···A	linked molecules	D−H (Å)	H···A (Å)	D···A (Å)	D−H···A (Å)	symmetry
m-OMe	C13--H13···O1	interchains	0.93	2.6	3.501(4)	164	−1+*x*,*y*,*z*

magnitude and are not expected to be the main cause for type affiliation.

Nonetheless, the types can clearly be distinguished when looking at the connectivity of each molecule. In types II and IV, each molecule is connected to four other ones, each intermolecular bond being formed with a different partner. While in type I, one molecule is linked to only two other molecules, two bonds being formed with the same partner. Consequently, types II and IV structures may be more difficult to form since it requires the concomitant approach of fives molecules, constrained by their mutual steric hindrance. In other words, type I structures seem kinetically favored in comparison with types II and IV structures.

On top, type IV is presumably less represented than types I and II because the H bonding motif present in this type does not seem to suit ortho- and para- derivatives. Indeed, a substituent in those positions would sterically hinder the approach of the adjacent molecules on the ladder and other neighboring ladders molecules.

Finally, type I structures present a particularly strong C−H···O intermolecular interaction (Table 4) between molecules of one ladder that may be evoked to justify its preponderance toward type II structures, which do not display this additional contact.

Hence it is reasonable to expect that crystallization of another derivative from this family of compounds would preferentially lead to a structure belonging to type I or II, with a slight preference for type I.

Other steric considerations can also be taken into account to further differentiate between types I and II. For example, one can easily understand that most structures with an ortho substituent do not belong to type I in which the substituent would be too close to the carbonyl of an adjacent ladder. Conversely, the o-Ph structure is part of type I instead of II because, in this case, the cavity occupied by the other ortho substituents in type II would be too small to accommodate the phenyl group.

One should however keep in mind, that for some compounds described here, it seems that different types would still be sterically allowed, and it is therefore not a straightforward task to predict the resulting type. Polymorphism of these compounds seems likely, especially for those having an alkyl/methoxy substituent on the benzylidene moeity. For example, one can easily imagine m-Me (type II), p-Me, and p-Ph (type III) in type I. Similarly, m-oMe could form an intramolecular N2--H2B···N1 bond rather than an intermolecular one and belong to another structure type. Unfortunately, the polymorphism investigation carried out so far to confirm this hypothesis did not lead to any of these alternative forms (Table 5).

CONCLUSION

In this contribution, the structural analysis of 20 compounds from the family of (S)-phenylglycine amide benzaldimines has been performed.

Paying attention only to strong hydrogen bonds (i.e., bonds in which the hydrogen is linked to a highly electronegative

DOI: 10.1021/acs.cgd.5b00621
Cryst. Growth Des. 2015, 15, 4005−4019

Table 5. Solvents[a] in Which a Single Crystal Was Successfully Grown and Polymorphs Identified for the 20 Compounds Sorted by Types

type	compounds	solvents of crystallization	polymorphs found in specified solvent
I	o-Ph	MeOH, ACN, EtAc	
	p-OMe	ACN, EtAc	
	p-F	MeOH, ACN, EtAc	
	p-Cl	MeOH, ACN, EtAc, DCM	
	p-Br	MeOH, EtAc	
	p-NO_2	ACN, EtAc	
	m-F	MeOH, EtAc, DCM	
	m-Cl	MeOH, ACN, EtAc	
	m-Br	MeOH, ACN	
	m-NO_2	MeOH, ACN	
II	m-Me	MeOH, DCM	
	o-Me	MeOH, ACN, EtAc	
	o-OMe	MeOH,ACN,EtAc,DCM	DCM: FII in type V
	o-F	MeOH, EtAc	
	o-Cl	MeOH, ACN, Ac	ACN: FI, Ac: FII, MeOH: FIII
	o-Br	MeOH, ACN, EtAc	
	o-NO_2	ACN, EtAc	
III	p-Me	MeOH, ACN, EtAc, DCM	
	p-Ph	MeOH, ACN, EtAc, DCM	
IV	m-OMe	MeOH, ACN	
V	o-OMe	MeOH, ACN, EtAc, DCM	MeOH: FI in type II

[a]MeOH: methanol, ACN: acetonitrile, EtAc: ethyl acetate, DCM: dichloromethane, Ac: acetone.

atom), it was possible to sort the 20 compounds into five types according to the hydrogen bonding pattern formed. In most structure types, the nature of the hydrogen bonds is similar, and the difference resides in their number and position (inter- or intramolecular) in the crystal.

We then performed a more thorough investigation of each type by considering secondary interactions. Some interactions inter- or intramotif (such as C−H···O ones) were found to be specific to certain types. But as far as C−H···π, π−π stacking, and other hydrophobic interactions are concerned, we noticed they vary considerably within a type and therefore do not seem to be responsible for type affiliation.

Our analysis reveals that there are three other factors that guide the formation of a specific motif and its preponderance over the other motifs:

1. the number of strong hydrogen bonds formed in the motif, which can include C−H···O contacts (thermodynamic considerations),
2. the ease with which the motif is formed, which is related to the coordination number of each molecule in the structure type (kinetic considerations),
3. the capacity of the motif to accommodate substituents on the different positions (ortho, meta, para) of the benzylidene, which is linked to the proximity of the molecules in the structure type (steric considerations).

By evoking those differences and some steric considerations, we were thus able to suggest a rationalization of the type allocation. According to our analysis, another derivative from this family of compounds would preferentially crystallize in type I or II, with a slight preference for type I.

However, it seems that for some compounds, especially the alkyl/methoxy derivatives, crystallization could reasonably lead to different outcomes. Polymorphism seems thus highly likely in this family of compounds.

Hence, despite much research ongoing in this area and with new analytical tools available, it appears that the rationalization and prediction of structures based on hydrogen-bonding patterns remain very much a challenge.

■ ASSOCIATED CONTENT

Supporting Information

Crystallographic information file. The Supporting Information is available free of charge on the ACS Publications website at DOI: 10.1021/acs.cgd.5b00621. Structures described in this contribution have been deposited at the Cambridge Crystallographic Data Centre and allocated the deposition numbers 1061022 for o-Ph, 1061023 for p-OMe, 1061024 for p-F, 1061025 for p-Cl, 1061026 for p-Br, 1061027 for p-NO_2, 1061028 for m-F, 1061029 for m-Cl, 1061030 for m-Br, 1061031 for m-NO_2, 1061043 for m-Me, 1061044 for o-Me, 1061045 for o-OMe FI, 1061046 for o-F, 1061047 for o-Cl FI, 1061048 for o-Cl FII, 1061049 for o-Cl FIII, 1061050 for o-Br, 1061051 for o-NO_2, 1061052 for p-Me, 1061053 for p-Ph, 1061054 for m-OMe, 1061055 for o-OMe FII.

■ AUTHOR INFORMATION

Corresponding Author

*Address: Institute of Condensed Matter and Nanosciences Molecules, Solids and Reactivity, Université Catholique de Louvain, Place Louis Pasteur 1, bte L4.01.03 B-1348 Louvain-La-Neuve, Belgium. Tel: +32 10 47 2811. Fax: +32 10 47 27 07. E-mail: tom.leyssens@uclouvain.be. Web: http://www.uclouvain.be/leyssens-group.

Notes

The authors declare no competing financial interest.

■ ACKNOWLEDGMENTS

The authors would like to thank the UCL, UNamur and FNRS (PDR T009913F, T016913, FRIA grant) for financial support, as well as T. Vergote for DFT calculations.

■ REFERENCES

(1) Shapiro, H. K. *Am. J. Ther.* **1998**, *5*, 323−353.
(2) Jin, X.-D.; Jin, Y.-H.; Zou, Z.-Y.; Cui, Z.-G.; Wang, H.-B.; Kang, P.-L.; Ge, C.-H.; Li, K. *J. Coord. Chem.* **2011**, *64*, 1533−1543.
(3) Shi, L.; Fang, R.-Q.; Zhu, Z.-W.; Yang, Y.; Cheng, K.; Zhong, W.-Q.; Zhu, H.-L. *Eur. J. Med. Chem.* **2010**, *45*, 4358−4364.
(4) Villar, R.; Encio, I.; Migliaccio, M.; Gil, M. J.; Martinez-Merino, V. *Bioorg. Med. Chem.* **2004**, *12*, 963−968.
(5) Abdel Aziz, A. A.; Salem, A. N. M.; Sayed, M. A.; Aboaly, M. M. *J. Mol. Struct.* **2012**, *1010*, 130−138.
(6) Lu, J.; Li, C.; Chai, Y.-F.; Yang, D.-Y.; Sun, C.-R. *Bioorg. Med. Chem. Lett.* **2012**, *22*, 5744−5747.
(7) Schmidt, M. F.; El-Dahshan, A.; Keller, S.; Rademann, J. *Angew. Chem., Int. Ed.* **2009**, *48*, 6346−6349.
(8) Kargar, H.; Jamshidvand, A.; Fun, H.-K.; Kia, R. *Acta Crystallogr., Sect. E: Struct. Rep. Online* **2009**, *65*, m403−m404.
(9) Yeap, C. S.; Kia, R.; Kargar, H.; Fun, H.-K. *Acta Crystallogr., Sect. E: Struct. Rep. Online* **2009**, *65*, m570−m571.
(10) Nozaki, H.; Takaya, H.; Moriuti, S.; Noyori, R. *Tetrahedron* **1968**, *24*, 3655−3669.
(11) Noorduin, W. L.; Izumi, T.; Millemaggi, A.; Leeman, M.; Meekes, H.; Van Enckevort, W. J. P.; Kellogg, R. M.; Kaptein, B.; Vlieg, E.; Blackmond, D. G. *J. Am. Chem. Soc.* **2008**, *130*, 1158−1159.

DOI: 10.1021/acs.cgd.5b00621
Cryst. Growth Des. 2015, 15, 4005−4019

(12) Noorduin, W. L.; Meekes, H.; van Enckevort, W. J. P.; Kaptein, B.; Kellogg, R. M.; Vlieg, E. *Angew. Chem., Int. Ed.* **2010**, *49*, 2539−2541.
(13) Noorduin, W. L.; Meekes, H.; van Enckevort, W. J. P.; Millemaggi, A.; Leeman, M.; Kaptein, B.; Kellogg, R. M.; Vlieg, E. *Angew. Chem., Int. Ed.* **2008**, *47*, 6445−6447.
(14) Noorduin, W. L.; Meekes, H.; Bode, A. a. C.; van Enckevort, W. J. P.; Kaptein, B.; Kellogg, R. M.; Vlieg, E. *Cryst. Growth Des.* **2008**, *8*, 1675−1681.
(15) Noorduin, W. L.; van Enckevort, W. J. P.; Meekes, H.; Kaptein, B.; Kellogg, R. M.; Tully, J. C.; McBride, J. M.; Vlieg, E. *Angew. Chem., Int. Ed.* **2010**, *49*, 8435−8438.
(16) Noorduin, W. L.; Van Der Asdonk, P.; Bode, A. A. C.; Meekes, H.; Van Enckevort, W. J. P.; Vlieg, E.; Kaptein, B.; Van Der Meijden, M. W.; Kellogg, R. M.; Deroover, G. *Org. Process Res. Dev.* **2010**, *14*, 908−911.
(17) Guo, H.-F.; Pan, Y.; Ma, D.-Y.; Lu, K.; Qin, L. *Transition Met. Chem.* **2012**, *37*, 661−669.
(18) Gül, Z. S.; Ersahin, F.; Agar, E.; Isik, S. *Acta Crystallogr., Sect. E: Struct. Rep. Online* **2007**, *63*, o2902.
(19) Kantar, E. N.; Köysal, Y.; Gümüs, S.; Agar, E.; Soylu, M. S. *Acta Crystallogr., Sect. E: Struct. Rep. Online* **2012**, *68*, o1587.
(20) Kargili, H.; Macit, M.; Alpaslan, G.; Kazak, C.; Erdönmez, A. *Acta Crystallogr., Sect. E: Struct. Rep. Online* **2012**, *68*, o3176.
(21) Pekdemir, M.; Isik, S.; Alaman Agar, A. *Acta Crystallogr., Sect. E: Struct. Rep. Online* **2012**, *68*, o2148.
(22) Vesek, H.; Kazak, C.; Alaman A\ugar, A.; Macit, M.; Soylu, M. S. *Acta Crystallogr., Sect. E: Struct. Rep. Online* **2012**, *68*, o2518.
(23) Kaur, G.; Panini, P.; Chopra, D.; Roy Choudhury, A. *Cryst. Growth Des.* **2012**, *12*, 5096−5110.
(24) Cruz-Cabeza, A. J.; Schwalbe, C. H. *New J. Chem.* **2012**, *36*, 1347.
(25) Etter, M. C.; MacDonald, J. C.; Bernstein, J. *Acta Crystallogr., Sect. B: Struct. Sci.* **1990**, *46*, 256−262.
(26) McKinnon, J. J.; Spackman, M. A.; Mitchell, A. S. *Acta Crystallogr., Sect. B: Struct. Sci.* **2004**, *60*, 627−668.
(27) Dalmolen, J.; van der Sluis, M.; Nieuwenhuijzen, J. W.; Meetsma, A.; de Lange, B.; Kaptein, B.; Kellogg, R. M.; Broxterman, Q. B. *Eur. J. Org. Chem.* **2004**, *2004*, 1544−1557.
(28) Sheldrick, G. M. *Acta Crystallogr., Sect. A: Found. Crystallogr.* **2008**, *64*, 112−122.
(29) Wood, P. A.; Olsson, T. S. G.; Cole, J. C.; Cottrell, S. J.; Feeder, N.; Galek, P. T. A.; Groom, C. R.; Pidcock, E. *CrystEngComm* **2013**, *15*, 65−72.
(30) Wolff, S. K.; Grimwood, D. J.; McKinnon, J. J.; Turner, M. J.; Jayatilaka, D.; Spackman, M. A. *CrystalExplorer*, version 3.1; University of Western Australia: Perth, 2012.
(31) Noorduin, W. L.; van der Asdonk, P.; Meekes, H.; van Enckevort, W. J. P.; Kaptein, B.; Leeman, M.; Kellogg, R. M.; Vlieg, E. *Angew. Chem., Int. Ed.* **2009**, *48*, 3278−3280.
(32) Leeman, M.; Noorduin, W. L.; Millemaggi, A.; Vlieg, E.; Meekes, H.; van Enckevort, W. J. P.; Kaptein, B.; Kellogg, R. M. *CrystEngComm* **2010**, *12*, 2051.
(33) Van Der Meijden, M. W.; Leeman, M.; Gelens, E.; Noorduin, W. L.; Meekes, H.; Van Enckevort, W. J. P.; Kaptein, B.; Vlieg, E.; Kellogg, R. M. *Org. Process Res. Dev.* **2009**, *13*, 1195−1198.
(34) Desiraju, G. R.; Murty, B. N.; Kishan, K. V. R. *Chem. Mater.* **1990**, *2*, 447−449.
(35) Lo Presti, L.; Soave, R.; Destro, R. *J. Phys. Chem. B* **2006**, *110*, 6405−6414.
(36) Etter, M. C. *J. Phys. Chem.* **1991**, *95*, 4601−4610.
(37) Galek, P. T. a; Chisholm, J. a; Pidcock, E.; Wood, P. a. *Acta Crystallogr., Sect. B: Struct. Sci., Cryst. Eng. Mater.* **2014**, *70*, 91−105.
(38) Bilton, C.; Allen, F. H.; Shields, G. P.; Howard, J. A. K. *Acta Crystallogr., Sect. B: Struct. Sci.* **2000**, *56*, 849−856.
(39) Galek, P. T. a.; Fábián, L.; Allen, F. H. *Acta Crystallogr., Sect. B: Struct. Sci.* **2010**, *66*, 237−252.
(40) Spek, A. L. *Acta Crystallogr., Sect. D: Biol. Crystallogr.* **2009**, *65*, 148−155.
(41) Taylor, R. *CrystEngComm* **2014**, *16*, 6852−6865.
(42) Wood, P. a.; Allen, F. H.; Pidcock, E. *CrystEngComm* **2009**, *11*, 1563−1571.

DOI: 10.1021/acs.cgd.5b00621
Cryst. Growth Des. 2015, 15, 4005−4019